Climate-Induced Landslides within the Larch Dominant Permafrost Zone of Central Siberia

Viacheslav I Kharuk[1,2,5], **Alexandr S Shushpanov**[1], **Sergei T Im**[1,2,3] **and Kenneth J Ranson**[4]

[1] Sukachev Forest Institute, Krasnoyarsk, 660036, Russia

[2] Siberian Federal University, Krasnoyarsk, 660041, Russia

[3] Siberian State Aerospace University, Krasnoyarsk, 660014, Russia

[4] NASA's Goddard Space Flight Center, Greenbelt, MD 20771, USA

[5] Correspondence author.

E-mail: kharuk@ksc.krasn.ru, alexandr01061987@gmail.com, stim@ksc.krasn.ru and kenneth.j.ranson@nasa.gov

Abstract

Climate impact on landslide occurrence and spatial patterns were analyzed within the larch-dominant communities associated with continuous permafrost areas of Central Siberia. We used high resolution satellite imagery (i.e. QuickBird, WorldView) to identify landslide scars over an area of 62000 km^2. Landslide occurrence was analyzed with respect to climate variables (air temperature, precipitation, drought index SPEI), and GRACE satellite derived equivalent of water thickness anomalies (EWTA). Landslides were found only on southward facing slopes, and the occurrence of landslides increased exponentially with increasing slope steepness. Lengths of landslides correlated positively with slope steepness. The observed upper elevation limit of landslides tended to coincide with the tree line. Observations revealed landslides occurrence was also found to be strongly correlated with August precipitation (r = 0.81) and drought index (r = 0.7), with June-July-August soil water anomalies (i.e., EWTA, r = 0.68–0.7), and number of thawing days (i.e., a number of days with t_{max} > 0°C; r = 0.67). A significant increase in the variance of soil water anomalies was observed, indicating that occurrence of landslides may increase even with a stable mean precipitation level. The key-findings of this study are (1) landslides occurrence increased within the permafrost zone of Central Siberia in the beginning of the 21st century; (2) the main cause of increased landslides occurrence are extremes in precipitation and soil water anomalies; and (3) landslides occurrence are strongly dependent on relief features such as southward facing steep slopes.

Keywords: permafrost in Siberia, larch forests, landslides, GRACE, landslides in permafrost, permafrost melting, landslides hazard

1. Introduction

Landslides are a widespread phenomenon within Eurasian and North American permafrost areas (Gorshkov *et al* 2003, Wieczorek *et al* 2007, Wang *et al* 2009, Jones *et al* 2010). As with other processes initiated by freeze–thaw cycles (e.g., Sturm *et al* 2005), landslides are enhanced by the considerable volumetric changes of water in the soil (Jones *et al* 2010). Studies have shown that in recent years warming in permafrost areas has resulted in an increase of landslide incidents, with landslides expected to be more frequent with continued warming temperature and an increase in precipitation (Montrasio and Valentino 2008, Blunden and Arndt 2011, Shan *et al* 2015).

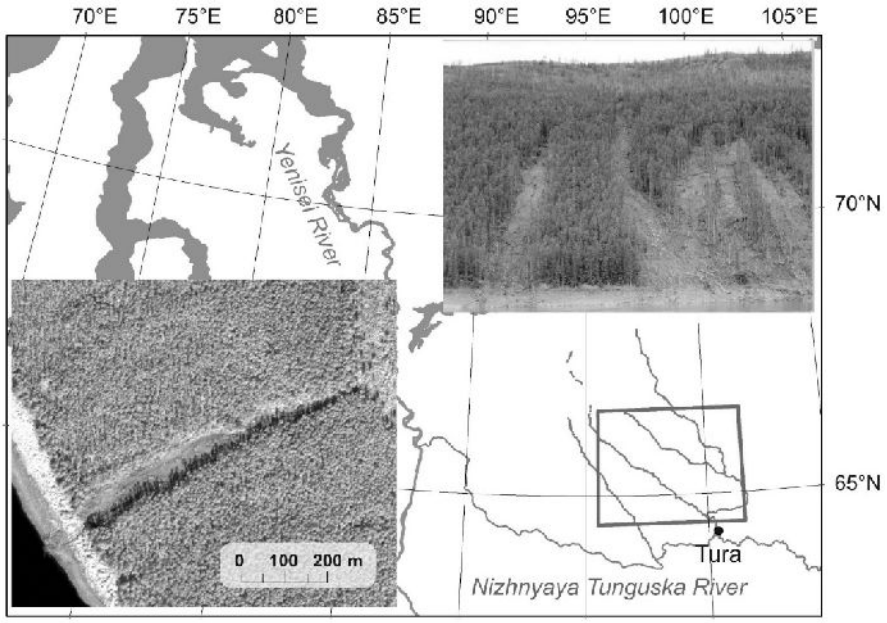

Figure 1. The study area covers about 62000 km^2 near Tura, Russia in northern Siberia as shown by the box. Insets: on-ground photo (above) and high-resolution satellite scene of a typical landslide.

Substantial reduction in the range of the geographical limits of permafrost has been observed since 1975 in Russia (IPCC 2013). During the last four decades, an increase of permafrost temperatures of 0.3–2.0°C has also been observed in Siberia (Romanovsky *et al* 2010). Temperature increases of 2°C or greater may impact local industrial infrastructure, including the gas and oil industries (Anisimov and Reneva 2011).

The region of interest for understanding landslides on permafrost is large, remote and well suited for satellite scenes analysis and GIS techniques (Huscroft *et al* 2003, Lyle *et al* 2004, Chau *et al* 2004, Booth *et al* 2009). Remote sensing of landslides in forested areas is based on change-detection using vegetation indices (e.g., EVI, NDVI), or detection of the denudation of landslide beds (Chau *et al* 2004, Booth *et al* 2009). Starting from 2002, GRACE (Gravity Recovery and Climate Experiment) satellite mission has provided estimates of the Earth's gravitational field anomalies resulting, in particular, from

change of water mass. GRACE data have been analyzed for water mass changes in the Arctic and Antarctic (Chen *et al* 2006, Gardner *et al* 2011, Barletta *et al* 2013, Groh *et al* 2014). GRACE data were also used in analysis of water mass changes in permafrost areas of Siberia and Alaska (Muskett and Romanovsky 2011a,b, Steffen *et al* 2012, Velicogna *et al* 2012). GRACE measurements could be applied for landslide studies because landslides are strongly connected with soil water content changes (Jones *et al* 2010).

The goal of the work reported herein was to (i) estimate spatial pattern of landslides and their dependence on terrain elevation and slope azimuth and steepness, (ii) discover if there is a dependence of landslide occurrence on climate variables (air temperature, precipitation and drought index) and gravimetric soil moisture as estimated from GRACE data.

2. Methods

2.1. Study area

The study area is located within the northern part of Central Siberia and includes the watershed of the Kochechum River including the Tembenchi and Embenchime tributaries. The area lies to the north and west of the small town of Tura and encompasses about 62000 km^2 (figures 1, 2). This site is with a portion of the Siberian Traps, a vast basaltic plateau dissected by many rivers. This is a hilly area with elevations ranging from 100 to 1100 m a.s.l. and permafrost thickness about 200-400 m. Active layer thickness is about 0.5–1.5 m within sediments and about 5 m within bedrocks (Ershov 1989). Sediments are composed of sandy and clay loams and contain about 10–30% of fragmented debris. Ground ice content within sediments on the slopes reached 10–15%. Kurums (rock fields) were found at the upper parts of the slopes. Solifluction processes are widespread within the area and observed mainly within the middle and lower part of slopes. Regularly, solifluction rates are low (about 1 mm yr^{-1}) (Ershov 1989). Trees within the solifluction zone deviate from the vertical direction and form so called “drunken forest”.

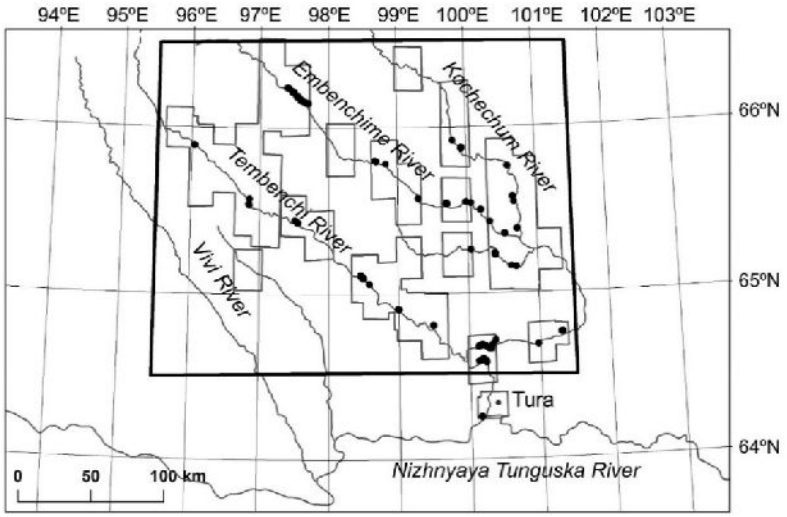

Figure 2. Study area shown by rectangle. Boxes within the study area indicate high spatial resolution image data. coverage.

The mean permafrost temperature was about -2 to -4°C on the middle and lower part of valleys, reaching -5 to -7°C at the highest elevations locations (Ershov 1989). Forests are formed by larch (*Larix gmelinii* Rupr.) with rare birch (*Betula pendula* Roth) admixture. The mean crown closure for larch stands was about 0.2. Mean height, diameter at breast height and age were 8.5 m, 12.5 cm and 250 years, respectively, based on sample plot measurements acquired in 2007 and 2012. Ground cover was composed of small shrubs (*Betula nana, Salix sp, Ribes sp, Rosa sp., Juniperus sp, Vaccinium sp*), lichen and moss. Soils are cryogenic brown soils (Ershov 1998).

2.2. Climate

Climate within the study area is strongly continental with long cold winters and short warm summers (table 1, figure 3). Recorded maximum July temperatures have reached +39°C. Snow melting is observed regularly during the month of May. Stable snow cover is formed beginning in early October. Mean snow depth is about 40-50 cm.

Table 1. Mean climate data (averaged for the period 1950-2013 for the study area

Variable	Annual	June-August	August
Mean temperature, °C	-16.6±0.3[a]	8.4±0.2	7.5±0.7
Mean sum of precipitation, mm	415.5±17	185.0±13	70.0±3

[a]confidence level p>0.05

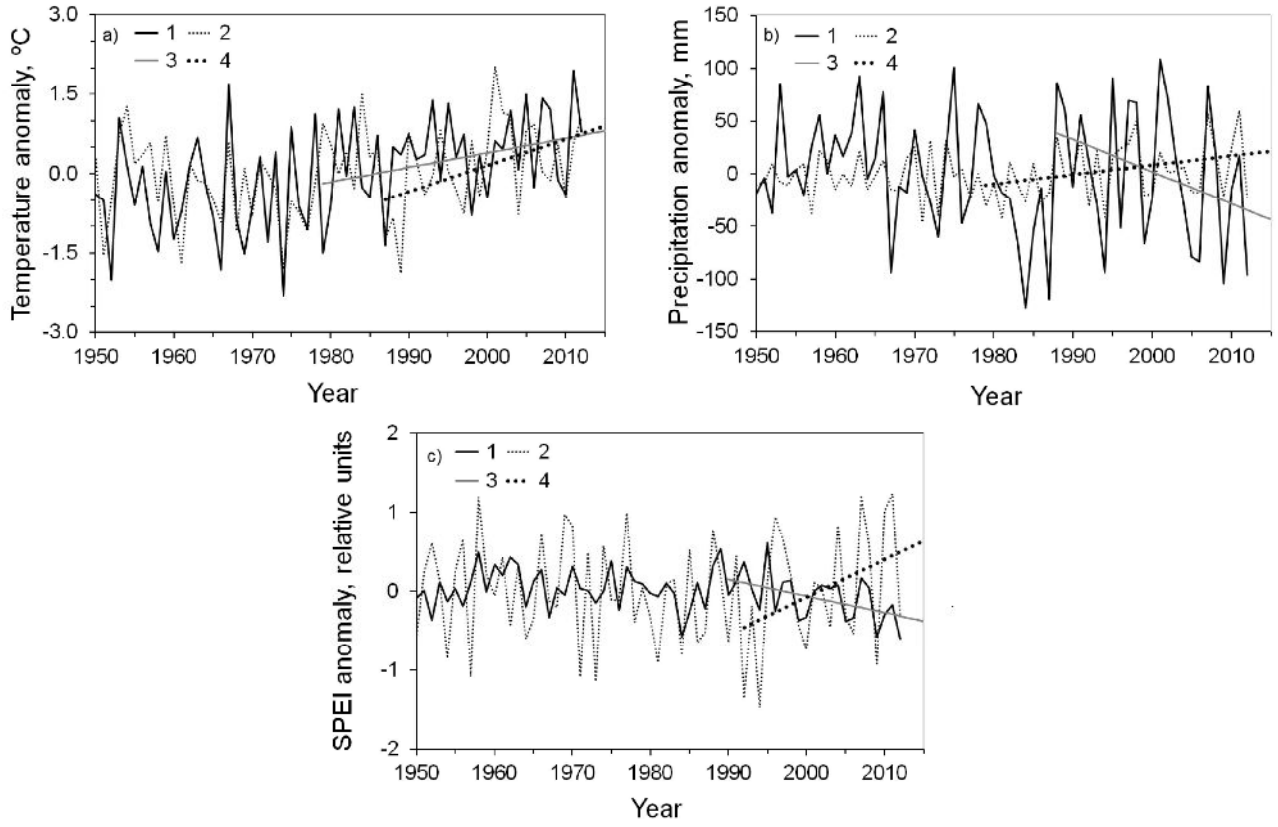

Figure 3. Climate variable anomalies within the study area (referenced to years 1950 to 2012): (a) temperature (1, 2 – annual and summer); (b) precipitation (1, 2 – annual and August), and (c) SPEI (1, 2 – annual and August). 3, 4 – trends ($p < 0.05$). Note: SPEI decrease indicates drought increase, and *vice verse*.

We used daily, monthly, summer and annual air temperature, and also sum of positive temperatures in June-July-August (JJA), May-June-July-August (MJJA) and May-June-July-August-September (MJJAS), mean summer temperatures, and the number of thawing days $N_{t>0}$ (i.e., number of days with positive temperatures: $t_{max} > 0$). Precipitation was analyzed as monthly and summer (i.e., JJA) values. In addition, a correlation of landslide occurrence with drought index SPEI was analyzed. The SPEI (the Standardized Precipitation-Evapotranspiration Index) can measure drought severity according to its intensity and duration (Vicente-Serrano *et al* 2010). The SPEI uses the monthly difference (D_i) between precipitation and PET (potential evapotranspiration): $D_i = P_i - PET_i$.

PET (mm) is obtained by:

$$PET = 16 \times K \times (10 \times T \times I^{-1})^m,$$

where T is the monthly mean temperature in °C; I is a heat index, which is calculated as the sum of 12 monthly index values, m is a coefficient depending on I, and K is a correction coefficient computed as a function of the latitude and month which takes into account number of sun hours in a day. SPEI data were

obtained from (http://sac.csic.es/spei/database.html) and averaged for a cell size 0.5°×0.5° (~33×56 km^2 at the study location).

Data (monthly and daily air temperature and precipitation) from the weather station at the nearby town of Tura (coordinates: 64.27 N. 100.23 E.) were used in the analysis (http://aisori.meteo.ru/ClimateR). Within the study area positive annual temperature trends were observed since the 1980s (figure 3a). An increase of August precipitation was observed since the 1990s, whereas annual precipitation decreased (figure 3b). A positive August drought index SPEI trend (i.e., drought decrease) has been observed since the 1990s (figure 3c).

2.3. Satellite data

WorldView-1, -2 and QuickBird-2 high-resolution (pixel size 0.5–0.6 m) scenes (Neigh *et al* 2013), Landsat-5, -7 panchromatic band (pixel size 15 m), and gravimetric measurements (GRACE, Gravity Recovery and Climate Experiment; http://www.csr.utexas.edu/grace) were used in this study. A time series of WorldView, QuickBird and Landsat scenes were compiled for landslide detection. High-resolution data (N = 110 summer-acquired scenes) covered the period 2004–2012. Each scene was corrected (i.e. geometry and radiometry corrections) and covered an area of 320 km^2 (with total analyzed area about 17500 km^2). These scenes (both black/white and spectral format) were used for landslide detection by manual photointerpretation. Landslides were identified based on texture and spectral characteristics and contextual information. The high quality of the WorldView-1, -2 and QuickBird-2 scenes used allowed very accurate detection of landslides (e.g., insert on figure 1, and figures 1-5 in Appendix). A digitizing tablet was used to measure length width and area of landslides. There were no misclassification with separating landslides from burned areas and other disturbances. On the other hand, precise dating of landslides was complicated by lack of high-resolution data for the period 2005–2008. That problem was solved by using Landsat scenes for the analysis, since for each year we have at least three Landsat scenes. Summer acquired, good quality Landsat scenes (N = 50) covered the period 1989–2012. For the period 1989–1999 only two scenes were available with the other 48 covering the period 2000–2012. Landsat scenes were obtained from USGS GloVis (http://glovis.usgs.gov).

GRACE data were used for soil water content estimation. We used annual and summer minimum and maximum gravimetric values, and equivalent of water thickness anomalies (EWTA, measured in cm). EWTA accuracy was approximately 10–30 mm month^{-1} (Riegger *et al* 2012; Long *et al* 2014). GRACE-derived EWTA values are caused by both water anomalies in the soil and in rivers and ponds. Because we used a watershed approach in this study, there was no incoming water flow from outside of the watershed. Because of that, EWTA is proportional to the soil water content anomalies. GRACE data are available since launch and activation in 2003 (http://grace.jpl.nasa.gov; Swenson and Wahr 2006, Landerer and Swenson 2012). GRACE spatial resolution was 1°×1° degree (~112×44 km^2 at latitude 66°). The data

were processed using ERDAS Imagine software (http://geospatial.intergraph.com) and ESRI ArcGIS software (http://www.esri.com).

2.4. GIS analysis

The distribution of landslides with respect to relief features (elevation, azimuth, slope steepness) was analyzed based on the ASTER global digital elevation model (DEM; http://earthexplorer.usgs.gov/). The ASTER DEM horizontal and vertical accuracy were ±20 m and ±30m, respectively (https://www.jspacesystems.or.jp/ersdac/GDEM/E/index.html). The elevation range was quantized to 50 m strata. Aspect and slope steepness data were calculated using DEM and ArcGIS tools. The aspect data were quantized to sixteen directions (i.e., by 22.5 degrees referenced clockwise from north). Because the distribution of relief features within the analyzed area was uneven, it could lead to bias. To avoid this, the data were normalized by the following procedure. The analyzed area with a given azimuth, slope steepness and elevation (shown by boxes on figure 2) was referenced to the total study area (rectangle on figure 2) with similar parameters:

$$K_{c(i)} = (A_{c(i)f} / A_{c(i)I}) * 100 \Big/ \sum_{i=a}^{b} (A_{c(i)f} / A_{c(i)I}), \qquad (1)$$

where $K_{c(i)}$ is the coefficient of normalization, *c(i)* is *i*-th category of landscape feature *c*, $A_{c(i)f}$ is the area of the given on-ground class within the *i*-th category of the topographic feature c, and $A_{c(i)I}$ is the area of the *i*-th category of topography feature *c* over the entire analyzed territory.

Statistical analysis of the data was carried out with Microsoft Excel and Statsoft Statistica (http://statsoft.ru) software. We used linear regression and Pearson correlation (*r*) analysis and Akaike information criterion (Akaike 1974) to determine significant relationships between landslides occurrence and climate variables and soil water anomalies (EWTA).

3. Results

3.1. Landslides statistics

Analysis of satellite imagery found that a total 145 landslides occurred during the time period from 2000 to 2012 within our study area. All of the observed landslides were used in the spatial analysis of landslides occurrence. Out of the total, 31 landslides were excluded from the temporal analysis because they could not be dated with one-year precision.

Figure 4a indicates that the number of landslides increased since 2006 with 80% occurring after 2006. The majority (60%) of landslides had lengths within the range of 75–225 m (figure 4b). The landslide statistics including slope azimuth (aspect) and slope steepness are presented in table 2.

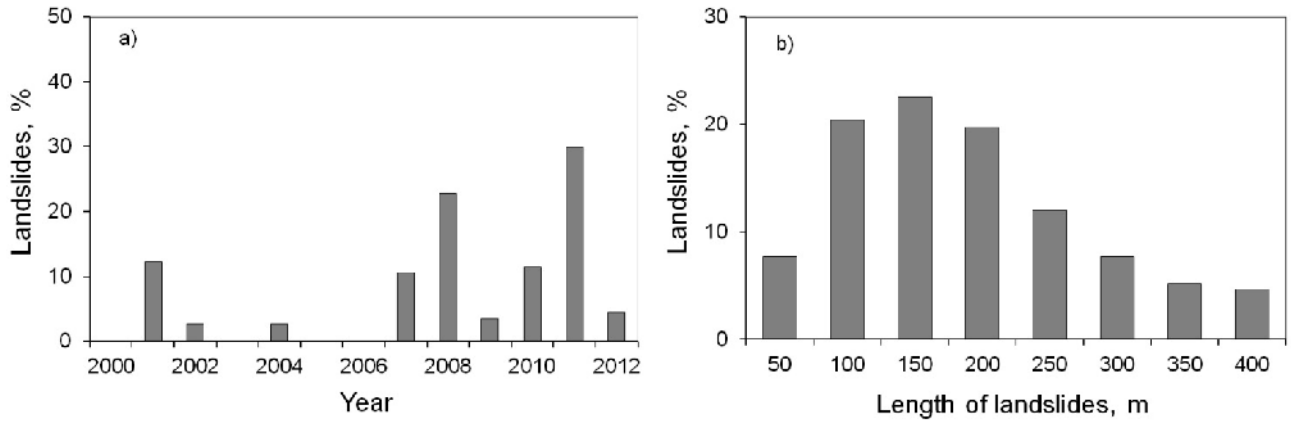

Figure 4. Landslide temporal dynamics (a) and length distribution (b).

Table 2. Landslide statistics.

	Landslide upper point elevation (m a.s.l.)	Azimuth, Degrees from North	Slope steepness (degrees)	Landslide width (m)	Landslide length (m)
Minimum value	150	67	2	15	10
Maximum value	600	293	40	60	400
Mean ± σ	340±110	225±40	22±10	36±15	170±95

3.2. Landslides and relief features

The spatial distribution of landslides is strongly uneven with respect to azimuth as seen in figure 6a. The majority of landslides occurred at slopes with southern and south-western exposures (figure 5a). With respect to elevation, most landslides had an upper limit mainly within the range of 200–300 m a.s.l. Occurrence of landslides declined exponentially as elevation increased (figure 5c). The maximal elevation of landslide initiation was found near the upper tree line, at about 650 m a.s.l. Landslides also exponentially increased with an increase in slope steepness (figure 5b). In figure 5d slope steepness is presented as sin(α), where α is the maximum slope angle along the extent of the landslide scar. There is a weak (but significant) positive correlation between landslide length and sin(α) (figure 5d).

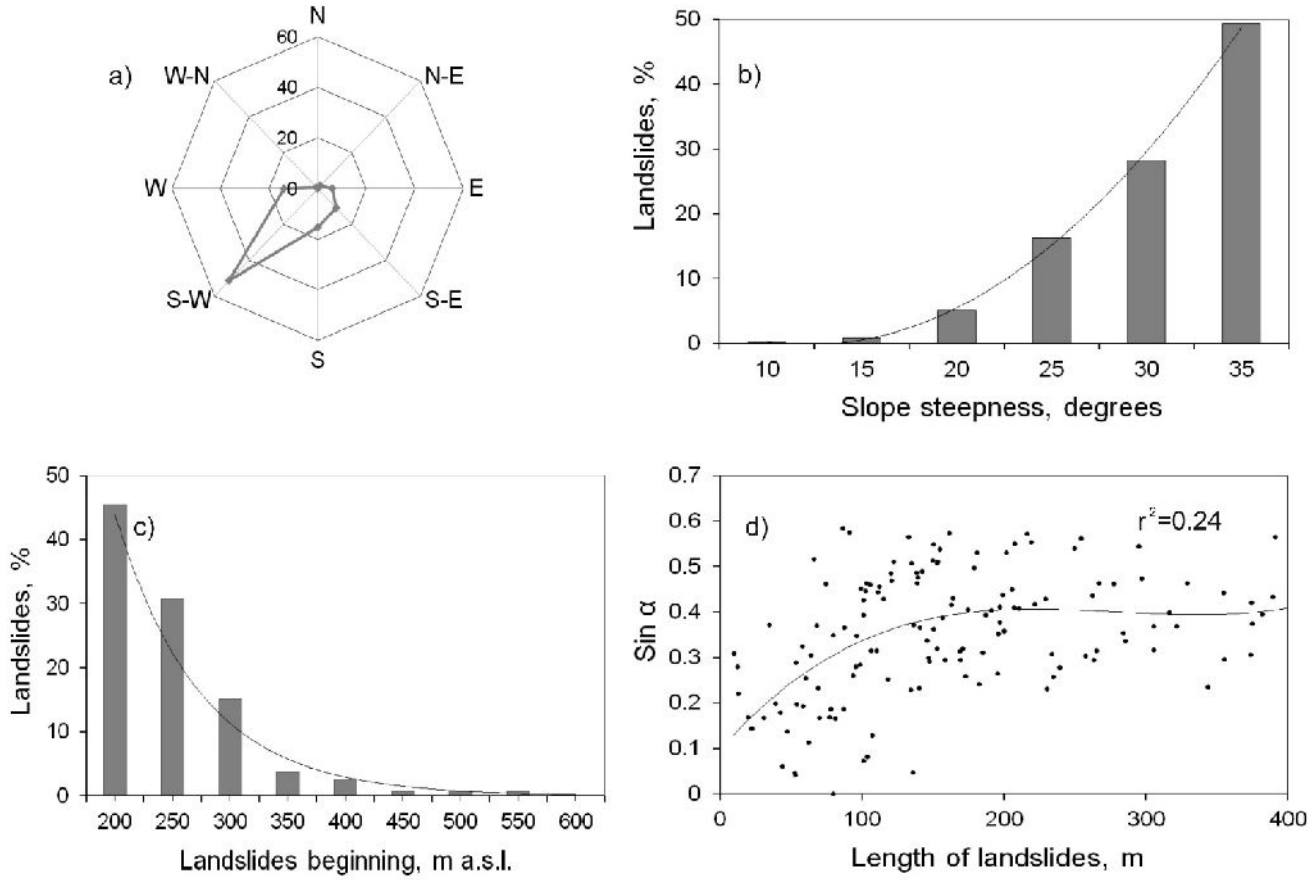

Figure 5. Relationship of landslides with relief features: (a) aspect (data were normalized based on equation (1), (b) slope steepness, (c) maximum elevation of landslides, and (d) landslides length dependence on sin(*a*) (*a* – maximum slope steepness along landslide track; trend is significant at $p < 0.05$).

3.3. Landslides and soil water content anomalies

Temporal dynamics of EWTA (equivalent of water thickness anomalies) coincided with landslide occurrence (figure 6a). A significant ($r^2 = 0.48$) correlation between landslides occurrence and June-August EWTA was observed (table 3, figure 6b). Note that a significant temporal increase of EWTA dispersion (i.e., soil water anomalies variation) extremes is observed (figure 6a). Drought index SPEI and soil water anomalies EWTA are correlated (figure 6c).

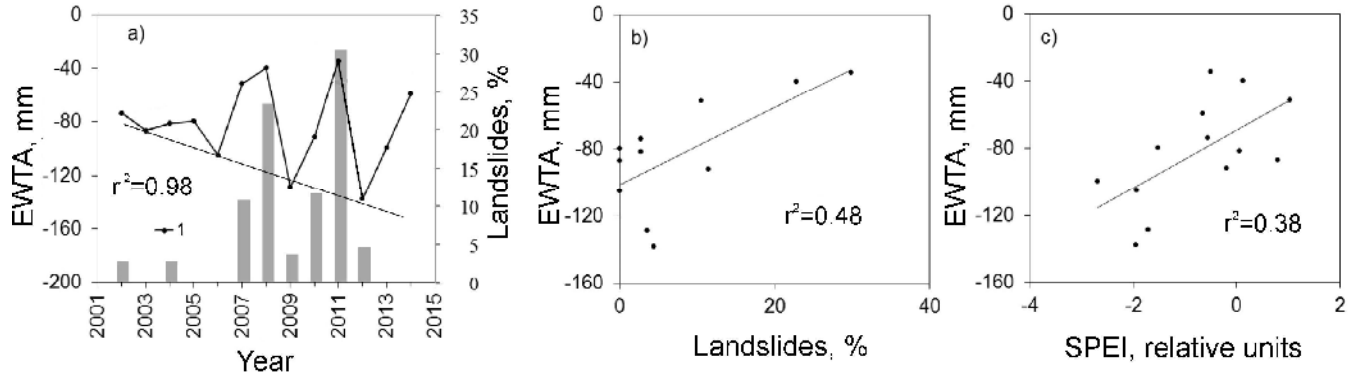

Figure 6. (a) Time series of August EWTA data are shown as solid black line (1). Trend of August EWTA minimum values shown by gray solid line ($p < 0.02$). Gray bars show landslides occurrence from figure 4a. (b) Landslide dependence on August EWTA (trend significant at p-level<0.02). (c) SPEI vs August EWTA data (trend significant at p-level<0.03). Note: SPEI decrease indicates drought increase, and *vice verse*.

3.4. Landslides and climate variables

Table 3 lists the correlation coefficients of climate variables and landslide occurrence. Landslide occurrence was found to be significantly correlated with annual mean temperatures ($r = 0.51$), but not annual precipitation. A higher correlation was observed with the $N_{t>0}$, duration of thawing period (i.e., number of days with $t_{max}>0°C$) ($r = 0.67$). The highest correlation was observed with August precipitation ($r = 0.81$). When averaged over the MJJA time period the correlation with precipitation was lower ($r = 0.58$). Correlations between SPEI drought index and landside occurrence were significant for July and August (table 3, figure 8b). Figures 7a and 7b shows observed positive linear relationships for August precipitation ($r^2 = 0.66$) and SPEI ($r^2 = 0.48$), respectively.

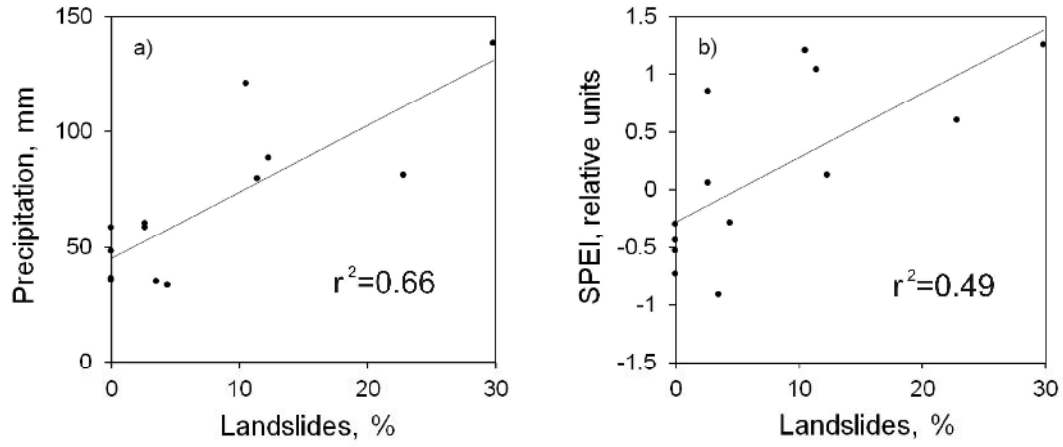

Figure 7. Relationship of landslide occurrence (%) with August precipitation (a) SPEI (b).

Table 3. Correlations of landslide occurrence with climate variables and EWTA.

	Pearson correlations (r_p)					
	Annual	May	June	July	August	MJJA
Precipitation	0.37	0.13	0.02	0.39	0.81[a]	0.58[a]
SPEI	0.37	-0.40	0.08	0.48[b]	0.70[a]	0.27
EWTA	0.54[b]	0.39	0.68[b]	0.70[a]	0.69[a]	
Temperature	0.37	51[b]	0.01	0.13	0.21	0.23
$N_{t>0}$ (thawing period)	0.67[a]	0.55[b]	-0.05	-0.36	0.02	0.67[a]
Σ (t°C >0)	0.20	0.52[b]	0.01	-0.38	0.05	0.21

[a], [b]– significant at $p < 0.05$ and $p < 0.1$, respectively.

4. Discussion

4.1. Landslides and relief features

The spatial pattern of landslides is uneven with respect to azimuth as all landslides occurred on slopes with the highest insolation and warmest temperatures, i.e. south and south-west facing slopes. Not a single landslide was found on the shadowed northern exposures. That effect is likely related to permafrost active layer depth. The latter varies from several cm to ≥1.0 m depending on exposure (Kharuk *et al* 2008). Landslide occurrence is also strongly dependent on slope steepness. The number of landslides increased exponentially with increases in slope steepness (figure 5c). Landslide lengths varied within a wide range – from short (≤50 m) to very long (>400 m) with a mean value about 170 m. The majority of landslides began at elevations between 200–250 m, with number decreasing exponentially with elevation increase (figure 4b). The maximum elevation of landslide headscarps approximates that of the upper tree line (which within the study area is about 650 m a.s.l.).

The presence of trees may promote landslide activation, because (1) the weight of trees provides a downslope driving force, and (2) tree roots help bind together the active layer. It is known that larch roots exist partly within the frozen soil horizon even during summer (Abaimov *et al* 2002). This occurs because (1) in anomalously warm years roots penetrate to deeper soil horizons and then are frozen in cold years, and (2) the active layer decreases from the moment of tree establishment. The latter is caused due to moss and lichen ground cover that acts as a thermal insulator (Kharuk *et al* 2008). Warming causes the active layer to increase, which releases the roots from the frozen soil. These, together with increased soil water content leads to the soil layer sliding over the permafrost while precipitation increases. The estimated landslide hazard area is about 30% of total area.

4.2. Landslides, climate variables and soil water anomalies

Landslides are significantly and positively correlated with July-August drought index and June -August soil water anomalies; thus, the probability of landslides increases as soil water anomalies increase (figure 6b). Globally, landslides were reported most frequently from July to September (Kirschbaum et al 2015), which coincided with our data with the exception of September. Meanwhile, there is a trend of increased variance of soil water anomalies (figure 6a). The latter indicates that the probability of a landslide occurring will increase even given a stable mean precipitation level. Landslides occurrence are significantly correlated with August precipitation (table 3, figure 6a). Notably, August precipitation increased during the last decade whereas the annual precipitation decreased (figure 3b). Moreover, precipitation itself increased active layer thickness due to high heat capacity of water (about four times in comparison with air). Along with precipitation, active layer thickness is significant for landslide occurrence. The active layer captures rainfall, and when pore water pressure is sufficient to reduce normal friction to a critical level, landslides can occur. The deeper active layer provides a higher rainfall trapping, increasing active layer weight over permafrost. The increasing probability of landslides triggering obeys Newton's Second Law (Iverson 2000). It is known that due to shallow active layer and no underlying permafrost permeability the majority of rainfall goes directly to the rivers. Along with rainfall, water seepage from thawing permafrost also increases the landslide probability. Significantly, landslides occurrence correlated positively not only with precipitation, but also with SPEI drought index (figure 7b). Thus, with a decrease in drought conditions landslides occurrence also increased.

No correlation was found between landslides occurrence and summer air temperatures. Meanwhile, landslides occurrence was significantly correlated ($r^2 = 0.67$) with the number of days with $t_{max} > 0°C$ ($N_{t>0}$) during the May-August period. Thus, the annual period of warming is a significant determinant of landslides occurrence. The main variability of $N_{t>0}$ was observed in May ($r^2 = 0.55$) Table 3), i.e. $N_{t>0}$ increase or decrease occurred during May depending on the year. Similarly, landslides occurrence was correlated with the sum of positive temperatures during May ($r^2 = 0.52$). This coincides with the general trend of climate warming, i.e. earlier snow melting.

A weak (and significant) correlation was observed with annual temperatures (table 3). That correlation may be a consequence of "permafrost warming". When permafrost temperature is increasing there is a decrease in shear and normal stresses of frozen ground due to less ice-bonding (there is particularly strong decrease from -3 to 0°C (Streletskiy *et al* 2012). Although there are no data on the permafrost temperature increase within the study area, Romanovsky *et al* (2010) showed an increase of permafrost temperatures of 0.3–2°C in Siberia during the last four decades.

Thus, the main cause of observed increase in landslide occurrence is an increase of precipitation and soil water anomalies. Climate scenarios forecast an increase of air temperature in the Arctic from 7°C to 11°C by the end of the 21st century (Sillmann *et al* 2013, Vaks *et al* 2013). This warming may lead to

increases in the permafrost active layer thickness and ultimately more landslides. The data obtained supports the hypothesis that landslides occurrence will be more frequent with warming and an increase in precipitation (Montrasio and Valentino 2008).

Along with heavy rainfall and permafrost thawing, forest fires can trigger landslides too. There is evidence of warming–induced higher fire frequency within the Siberian permafrost zone (Kharuk *et al* 2011). According to predictions, a future increase of forest fires within the boreal zone is expected (e.g., Flannigan *et al* 1998), which in combination with permafrost thawing should increase the occurrence of landslides.

4.3. Post-landslides vegetation growth

Landslides create patches of disturbed soil that are the initiation of succession of forest species, including potential establishment of new species into the larch habitat. This problem has been addressed in only a few papers (e.g, Abaimov *et al* 2002). In particular, landslides scars present opportunities for establishment of less cold-tolerant species into larch-dominated forests. There is evidence of Siberian pine (*Pinus sibirica*) and fir (*Abies sibirica*) migration into larch-dominated communities (Kharuk *et al* 2005). In general post-landslide vegetation growth in permafrost is poorly understood and needs more investigation.

5. Conclusion

Based on the analysis of high-resolution satellite images and climate data for the period from 2000 to 2012, landslides have increased within the study area, an area of continuous permafrost in Central Siberia. This phenomenon correlates with August precipitation, drought decrease, and soil water anomalies. The main cause of the observed landslide occurrence increase is an increase of precipitation and soil water anomaly extremes. Landslide occurrence is strongly dependent on relief features and were found in the study to be located on southward facing slopes only on steeper slopes. The area studied represents the vast larch forests of the Central Siberian Plateau. We will expand our analysis to other parts of the Arctic forest and tundra to more fully understand the impacts of landslide dynamics on Arctic ecosystems and carbon balance.

Acknowledgements

Russian Science Foundation (grant #14-24-00112) primarily supported this research. Additional support for K. J. Ranson by NASA's Terrestrial Ecology program. GRACE land data were preprocessed by Sean Swenson, supported by the NASA MEaSUREs Program, and are available at http://grace.jpl.nasa.gov. DigitalGlobe data were provided by NASA's NGA Commercial Archive Data (cad4nasa.gsfc.nasa.gov) under the National Geospatial-Intelligence Agency's NextView license agreement.

References

Abaimov A P, Zyryanova O A and Prokushkin S G 2002 Long-Term Investigation of Larch Forests in Cryolithic Zone of Siberia: Brief History, Recent Results and Possible Changes under Global Warming *Eurasian Journal of Forest Research* 5 95

Akaike H 1974 A new look at the statistical model identification *IEEE Transactions on Automatic Control* 19 716–723

Anisimov O A and Reneva S A 2011 Carbon balance in the permafrost zone of Russia and the global climate: current status and forecast based on modeling *Polar cryosphere land and water* 320.

Barletta V R, Sorensen L S and Forsberg R 2013 Scatter of mass changes estimates at basin scale for Greenland and Antarctica *The Cryosphere* 7 1411–1432

Blunden J and Arndt D S 2011 State of the Climate in 2011 *American Meteorological Societ*y (http://www.ncdc.noaa.gov/bams-state-of-the-climate)

Booth A M, Roering J J and Perron J T 2009 Automated landslide mapping using spectral analysis and high-resolution topographic data: Puget Sound lowlands, Washington, and Portland Hills, Oregon *Geomorphology* 109 132–147

Chau K T, Sze Y L, Fung M K, Wong W Y, Fong E L and Chan L C P 2004 Landslide hazard analysis for Hong Kong using landslide inventory and GIS *Computers & Geosciences 30* 429–443

Chen J L, Wilson C R, Blankenship D D and Tapley B D 2006 Antarctic mass rates from GRACE *Geophysical Research Letters* 33 L11502

Ershov E D (ed) 1989 Geocryology of USSR. Middle Siberia, Nedara Publishing House, Moscow (in Russian)

Ershov Yu I 1998 Soil-geographical regionalization of the Krasnoyarsk Territory *Geography and natural resources* 2 110–118 (in Russian)

Gardner A S, Moholdt G, Wouters B, Wolken G J, Burgess D O, Sharp M J, Cogley J G, Braun C and Labine C 2011 Sharply increased mass loss from glaciers and ice caps in the Canadian Arctic Archipelago *Nature* 473 357–360

Gorshkov S P, Vandenberg J, Alekseev B A, Mochalova O I and Tishkova M A 2003 Climate, Permafrost and Landscapes of the Middle Yenisei Region, Nauka, Moscow (in Russian)

Groh A, Ewert H, Rosenau R, Fagiolini E, Gruber C, Floricioiu D, Abdel Jaber W, Linow S, Flechtner F, Eineder M and Dierking W 2014 Mass, Volume and Velocity of the Antarctic Ice Sheet: Present-Day Changes and Error Effects *Surveys in Geophysics* 35(6) 1481–1505

Flannigan M D, Bergeron Y, Engelmark O and Wotton B M 1998 Future wildfire in circumboreal forests in relation to global warming *J. Veg. Sci.* 9 469–476

Huscroft C A, Lipovsky P S and Bond J D 2003 Permafrost and landslide activity: Case studies from southwestern Yukon Territory *Yukon exploration and geology* 107–119

Jones A, Stolbovoy V, Tarnocai C, Broll G, Spaargaren O and Montanarella L (eds.) 2010 Soil Atlas of the Northern Circumpolar Region European Commission, Office for Official Publications of the European Communities, Luxembourg

IPCC 2013 *Climate Change 2013: The Physical Science Basis. Contribution of Working Group I to the Fifth Assessment Report of the Intergovernmental Panel on Climate Change* Cambridge ed T Stoker, D Qin, G Plattner, M Tignor, S Allen, J Boschung, A Nauels, Y Xia, V Bex and P Midgley (Cambridge: Cambridge University Press)

Iverson R M 2000 Landslide triggering by rain infiltration *Water Resources Research* 36(7) 1897–1910

Kirschbaum D, Stanley T and Zhou Y 2015 Spatial and temporal analysis of a global landslide catalog *Geomorphology* 249 4–15

Kharuk V I, Dvinskaya M L, Im S T and Ranson K J 2005 Expansion of Evergreen Conifers to the Larch-Dominated Zone and Climatic Trends *Russian Journal of Ecology* 36 164–170

Kharuk V I, Ranson K J and Dvinskaya M L 2008 Wildfires dynamic in the larch dominance zone *Geophys. Res. Lett*. 35 ARTN L01402

Kharuk V I, Dvinskaya M L, Im S T and Ranson K J 2011 Wildfires in northern Siberian larch dominated communities *Environmental Research Letters* 6(4)

Landerer F W and Swenson S C 2012 Accuracy of scaled GRACE terrestrial water storage estimates *Water Resources Research* 48 W04531

Long D, Longuevergne L and Scanlon B R 2014 Uncertainty in evapotranspiration from land surface modeling, remote sensing, and GRACE satellites *Water Resources Research* 50(2) 1131–1151

Lyle R R, Hutchinson D J and Preston Y 2004 Landslide processes in discontinuous permafrost, Little Salmon Lake (NTS 105L/1 and 2), south-central Yukon *Yukon exploration and geology* 193–204

Montrasio L and Valentino R 2008 A model for triggering mechanisms of shallow landslides *Natural Hazards and Earth System Sciences* 8 1149–1159

Muskett R R and Romanovsky V E 2011a Article Alaskan Permafrost Groundwater Storage Changes Derived from GRACE and Ground Measurements *Remote Sensing* 3 378–397

Muskett R R and Romanovsky V E 2011b Energy and mass changes of the Eurasian permafrost regions by multi-satellite and in-situ measurements *Natural Science* 3(10) 827–836

Neigh C S, Masek J G and Nickeson J E 2013 High-resolution satellite data open for government research *Eos, Transactions American Geophysical Union* 94(13) 121–123

Riegger J, Tourian M, Devaraju B and Sneeuw N 2012 Analysis of grace uncertainties by hydrological and hydro-meteorological observations *J. Geodyn.* 59 16–27

Romanovsky V E, Drozdov D S, Oberman N G, Malkova G V, Kholodov A L, Marchenko S S, Moskalenko N G, Sergeev D O, Ukraintseva N G, Abramov A A, Gilichinsky D A and Vasiliev A A 2010 Thermal state of permafrost in Russia *Permafrost Periglacial Process* 21 136–155

Shan W, Hu Z, Guo Y, Zhang C, Wang C, Jiang H, Liu Y and Xiao J 2015 The impact of climate change on landslides in southeastern of high-latitude permafrost regions of China *Front. Earth Sci*. 24

Sillmann J, Kharin V V, Zwiers F W, Zhang X and Bronaugh D 2013 Climate extremes indices in the CMIP5 multimodel ensemble: Part 2. Future climate projections *Journal of Geophysical Research: Atmospheres* 118 2473–2493

Steffen H, Muller J and Peterseim N 2012 Mass Variations in the Siberian Permafrost Region from GRACE *Geodesy for Planet Earth, International Association of Geodesy Symposia* 136 597–603

Streletskiy D A, Shiklomanov N I and Nelson F E 2012 Permafrost, infrastructure and climate change: A GIS-based landscape approach to geotechnical modeling *Arctic, Antarctic and Alpine Research* 44(3) 368–380.

Sturm M, Schimel J, Michaelson G, Welker J M, Oberbauer S F, Liston G E and Romanovsky V E 2005 Winter biological processes could help convert arctic tundra to shrubland *Bioscience* 55(1) 17–26

Swenson S C and Wahr J 2006 Post-processing removal of correlated errors in GRACE data *Geophysical Research Letters* 33 L08402

Vaks A, Gutareva O S, Breitenbach S F M, Avirmed E, Mason A J, Thomas A L, Osinzev A V, Kononov A M and Henderson G M 2013 Speleothems Reveal 500,000-Year History of Siberian Permafrost *Science* 340 183–186

Velicogna I, Tong J, Zhang T and Kimball J S 2012 Increasing subsurface water storage in discontinuous permafrost areas of the Lena River basin, Eurasia, detected from GRACE *Geophysical Research Letters* 39 L09403

Vicente-Serrano S M, Beguería S and López-Moreno J I 2010 A Multiscalar Drought Index Sensitive to Global Warming. The Standardized Precipitation Evapotranspiration Index *Journal Climate* 23 1696–1718

Wang B, Li H and Paudel B 2009 Movement behavior of thaw flows in permafrost soil Geohazard (http://www.landslides.ggl.ulaval.ca/geohazard/Processus/wang.pdf)

Wieczorek E L, Gerald F, Geist R, Motyka J and Matthias J 2007 Hazard assessment of the Tidal Inlet landslide and potential subsequent tsunami, Glacier Bay National Park, Alaska *Landslides* 4 (3) 205–215

Appendix

1. Landslides statistic

Table A1. Landslides data.

No.	Length (м)	Year	Landslides headscarp (m a.s.l.)	Slope steepness (°) (max)	Aspect (°) (mean)	Center point coordinates of the landslide	
						Longitude	Altitude
1	136	n/a	311	3	198	96° 2’25" E	65° 53’38" N
2	118	2001	170	15	127	100° 7’27" E	64° 41’1" N
3	141	2010	177	13	119	100° 7’22" E	64° 40’59" N
4	134	2011	178	13	131	100° 7’20" E	64° 40’59" N
5	106	2011	178	27	180	100° 10’53" E	64° 41’23" N
6	121	2011	183	28	188	100° 10’57" E	64° 41’23" N
7	139	2011	191	29	186	97° 29’32" E	66° 12’49" N
8	111	2011	185	27	188	100° 11’20" E	64° 41’21" N
9	112	2011	191	27	191	100° 11’23" E	64° 41’20" N
10	142	2011	198	30	190	100° 11’28" E	64° 41’20" N
11	135	2011	203	31	191	100° 11’31" E	64° 41’20" N
12	153	2011	218	30	202	97° 24’40" E	66° 14’10" N
13	54	2011	151	11	201	100° 13’8" E	64° 40’59" N
14	60	2002	158	15	175	100° 16’9" E	64° 40’10" N
15	53	2004	160	17	181	96° 50’33" E	65° 32’38" N
16	64	2004	161	18	181	100° 16’24" E	64° 40’8" N
17	58	2004	158	20	208	100° 16’14" E	64° 40’9" N
18	200	2002	199	21	143	100° 21’42" E	64° 43’3" N
19	297	2011	210	28	238	100° 13’37" E	64° 35’9" N
20	374	n/a	260	25	147	97° 28’22" E	66° 13’2" N
21	317	n/a	280	24	170	100° 10’43" E	64° 36’11" N
22	197	n/a	203	25	208	97° 39’56" E	66° 9’6" N
23	123	2012	217	31	236	100° 13’3" E	64° 35’43" N
24	150	2012	170	31	235	100° 12’57" E	64° 35’40" N
25	155	2012	193	33	230	100° 13’4" E	64° 35’36" N
26	216	2012	246	35	241	100° 13’16" E	64° 35’33" N
27	161	2012	255	35	235	100° 13’23" E	64° 35’32" N
28	355	2007	226	17	153	97° 36’0" E	66° 9’49" N
29	80	2011	158	2	184	100° 17’30" E	64° 40’7" N
30	66	2011	201	32	94	100° 18’60" E	64° 41’31" N
31	20	n/a	236	10	198	97° 31’46" E	65° 26’35" N
32	31	n/a	232	10	182	97° 32’7" E	65° 26’30" N
33	13	n/a	241	13	200	97° 31’9" E	65° 26’44" N
34	12	n/a	239	16	207	97° 30’50" E	65° 26’49" N
35	10	n/a	246	18	208	97° 30’39" E	65° 26’51" N
36	99	n/a	287	17	154	96° 51’9" E	65° 34’35" N
37	80	2011	278	21	180	98° 41’28" E	65° 47’56" N
38	35	n/a	266	22	207	98° 49’25" E	65° 47’8" N
39	44	2008	253	4	250	96° 50’35" E	65° 32’36" N

No.	Length (м)	Year	Landslides headscarp (m a.s.l.)	Slope steepness (°) (max)	Aspect (°) (mean)	Center point coordinates of the landslide	
						Longitude	Altitude
40	70	2008	261	10	279	96° 50’ 47" E	65° 32’ 27" N
41	285	2011	455	20	251	97° 32’ 35" E	66° 11’ 16" N
42	136	2011	452	22	242	97° 32’ 48" E	66° 11’ 9" N
43	211	2011	467	24	225	97° 32’ 57" E	66° 11’ 5" N
44	101	2011	448	25	217	97° 33’ 1" E	66° 11’ 4" N
45	202	2011	466	33	218	97° 33’ 2" E	66° 11’ 2" N
46	250	2011	454	33	218	97° 33’ 3" E	66° 10’ 59" N
47	120	2011	447	29	230	97° 33’ 9" E	66° 10’ 60" N
48	101	2011	432	23	226	97° 33’ 13" E	66° 10’ 58" N
49	229	2011	466	25	231	97° 33’ 14" E	66° 10’ 57" N
50	277	2011	451	27	225	97° 33’ 15" E	66° 10’ 56" N
51	103	2011	449	28	219	97° 33’ 23" E	66° 10’ 55" N
52	91	2011	449	36	225	97° 33’ 33" E	66° 10’ 51" N
53	99	2011	444	27	219	97° 33’ 25" E	66° 10’ 54" N
54	450	2008	572	31	209	97° 35’ 59" E	66° 9’ 57" N
55	295	2008	509	33	224	97° 35’ 49" E	66° 9’ 59" N
56	219	2008	515	34	222	97° 35’ 49" E	66° 10’ 3" N
57	150	2008	501	33	258	97° 35’ 38" E	66° 10’ 9" N
58	87	2008	481	36	247	97° 35’ 36" E	66° 10’ 10" N
59	267	2008	464	28	227	97° 35’ 58" E	66° 9’ 52" N
60	153	2008	452	31	228	100° 11’ 43" E	64° 41’ 18" N
61	254	2008	461	34	205	97° 36’ 45" E	66° 9’ 38" N
62	207	2008	471	34	204	100° 10’ 12" E	64° 41’ 27" N
63	248	2002	471	43	222	97° 36’ 23" E	66° 9’ 44" N
64	355	2008	464	26	231	100° 7’ 37" E	64° 35’ 31" N
65	157	2008	410	23	218	97° 36’ 10" E	66° 9’ 45" N
66	222	2007	484	25	183	97° 41’ 28" E	66° 8’ 51" N
67	164	2007	452	26	182	97° 41’ 37" E	66° 8’ 48" N
68	174	2007	423	24	168	97° 41’ 56" E	66° 8’ 47" N
69	163	2007	428	25	168	97° 41’ 54" E	66° 8’ 47" N
70	205	2007	456	27	194	97° 41’ 15" E	66° 8’ 49" N
71	115	2008	451	25	196	97° 41’ 13" E	66° 8’ 51" N
72	196	n/a	444	21	229	98° 59’ 53" E	64° 54’ 34" N
73	151	n/a	437	21	219	97° 40’ 10" E	66° 9’ 1" N
74	329	2008	468	28	215	97° 24’ 4" E	66° 14’ 17" N
75	375	2008	457	22	224	97° 23’ 54" E	66° 14’ 19" N
76	169	2008	444	18	245	97° 23’ 46" E	66° 14’ 27" N
77	185	2008	454	18	211	97° 24’ 16" E	66° 14’ 16" N
78	159	2008	452	17	238	97° 24’ 21" E	66° 14’ 16" N
79	110	2009	456	18	198	97° 24’ 36" E	66° 14’ 13" N
80	153	2009	438	19	208	97° 35’ 58" E	66° 9’ 54" N
81	322	2009	449	22	195	97° 24’ 51" E	66° 14’ 6" N
82	106	2009	444	18	195	97° 24’ 50" E	66° 14’ 9" N
83	382	2008	462	24	217	97° 29’ 7" E	66° 12’ 51" N
84	139	2008	460	28	211	100° 11’ 6" E	64° 41’ 23" N
85	197	2008	473	22	229	100° 11’ 23" E	64° 36’ 10" N

No.	Length (м)	Year	Landslides headscarp (m a.s.l.)	Slope steepness (°) (max)	Aspect (°) (mean)	Center point coordinates of the landslide	
						Longitude	Altitude
86	191	2008	472	24	207	97° 28’ 49" E	66° 12’ 59" N
87	147	2008	445	17	216	100° 41’ 24" E	65° 9’ 30" N
88	374	2008	443	18	204	100° 11’ 4" E	64° 36’ 12" N
89	94	2010	276	15	184	100° 35’ 49" E	65° 45’ 51" N
90	96	2001	282	20	149	100° 37’ 11" E	65° 9’ 48" N
91	87	2001	278	22	133	99° 56’ 1" E	65° 52’ 38" N
92	68	2001	272	22	152	100° 39’ 55" E	65° 34’ 51" N
93	78	2001	215	11	186	100° 19’ 22" E	65° 25’ 57" N
94	173	n/a	239	15	165	100° 32’ 7" E	65° 21’ 27" N
95	183	n/a	241	15	181	100° 32’ 5" E	65° 21’ 27" N
96	196	n/a	246	16	171	100° 31’ 59" E	65° 21’ 28" N
97	344	2007	403	14	71	100° 23’ 28" E	65° 13’ 59" N
98	231	2007	363	13	87	100° 23’ 31" E	65° 14’ 12" N
99	263	2007	366	17	71	100° 23’ 30" E	65° 14’ 17" N
100	257	2007	372	18	67	100° 23’ 29" E	65° 14’ 18" N
101	234	2007	375	18	72	100° 23’ 25" E	65° 14’ 21" N
102	235	2007	373	15	55	100° 23’ 18" E	65° 14’ 29" N
103	96	n/a	331	16	190	100° 39’ 50" E	65° 34’ 50" N
104	147	2001	310	18	191	97° 28’ 32" E	66° 13’ 3" N
105	104	2001	251	6	271	99° 17’ 55" E	65° 34’ 39" N
106	47	n/a	326	8	255	98° 59’ 27" E	64° 54’ 37" N
107	59	n/a	325	11	248	99° 48’ 25" E	65° 55’ 20" N
108	101	n/a	334	5	291	99° 56’ 2" E	65° 52’ 45" N
109	77	n/a	335	10	316	99° 55’ 53" E	65° 52’ 17" N
110	87	n/a	342	11	221	100° 39’ 38" E	65° 34’ 47" N
111	77	n/a	197	55	279	99° 56’ 2" E	65° 52’ 40" N
112	39	2010	224	13	229	99° 59’ 11" E	65° 33’ 10" N
113	22	2010	221	10	235	99° 59’ 12" E	65° 33’ 9" N
114	106	n/a	352	2	250	100° 2’ 35" E	65° 15’ 54" N
115	181	n/a	241	32	133	101° 18’ 7" E	64° 45’ 27" N
116	107	n/a	182	8	132	101° 18’ 48" E	64° 45’ 37" N
117	405	2010	332	27	206	100° 43’ 1" E	65° 23’ 11" N
118	221	2001	280	38	227	98° 27’ 30" E	65° 6’ 55" N
119	53	2010	252	3	260	100° 16’ 21" E	64° 40’ 9" N
120	52	n/a	230	3	221	99° 48’ 23" E	65° 55’ 21" N
121	391	n/a	277	35	147	100° 8’ 47" E	64° 15’ 23" N
122	146	2011	195	20	134	100° 9’ 30" E	64° 41’ 25" N
123	207	2011	220	24	176	97° 36’ 35" E	66° 9’ 42" N
124	179	2011	219	30	179	100° 10’ 34" E	64° 41’ 26" N
125	69	2010	265	14	220	96° 51’ 6" E	65° 32’ 18" N
126	42	n/a	233	11	221	100° 40’ 36" E	65° 32’ 54" N
127	170	2010	459	17	202	97° 24’ 32" E	66° 14’ 13" N
128	171	2010	464	19	216	97° 24’ 29" E	66° 14’ 15" N
129	262	2001	473	26	202	97° 28’ 55" E	66° 12’ 57" N
130	265	2001	380	18	226	100° 3’ 19" E	65° 32’ 45" N
131	187	2001	458	23	231	97° 32’ 53" E	66° 11’ 6" N

No.	Length (м)	Year	Landslides headscarp (m a.s.l.)	Slope steepness (°) (max)	Aspect (°) (mean)	Center point coordinates of the landslide	
						Longitude	Altitude
132	103	2011	446	27	218	97° 33’ 21" E	66° 10’ 55" N
133	75	2011	439	28	219	97° 33’ 20" E	66° 10’ 57" N
134	138	2011	468	29	223	97° 33’ 15" E	66° 11’ 0" N
135	133	2010	510	34	215	97° 36’ 1" E	66° 9’ 59" N
136	389	2010	462	26	224	97° 36’ 2" E	66° 9’ 50" N
137	199	2008	449	26	199	97° 28’ 41" E	66° 13’ 3" N
138	141	2011	383	21	189	98° 40’ 19" E	65° 48’ 11" N
139	240	n/a	369	16	196	99° 42’ 48" E	65° 32’ 33" N
140	305	n/a	406	22	186	100° 11’ 50" E	65° 30’ 14" N
141	400	2001	424	23	194	99° 42’ 21" E	65° 32’ 37" N
142	284	2001	420	21	215	99° 41’ 53" E	65° 32’ 48" N
143	305	2001	439	19	198	99° 42’ 37" E	65° 32’ 36" N
144	63	2010	252	7	245	96° 50’ 31" E	65° 32’ 39" N
145	81	2010	254	10	170	96° 50’ 30" E	65° 32’ 40" N

1

2. Samples of zoomed high-resolution scenes of landslieds (Figures A1-A5)

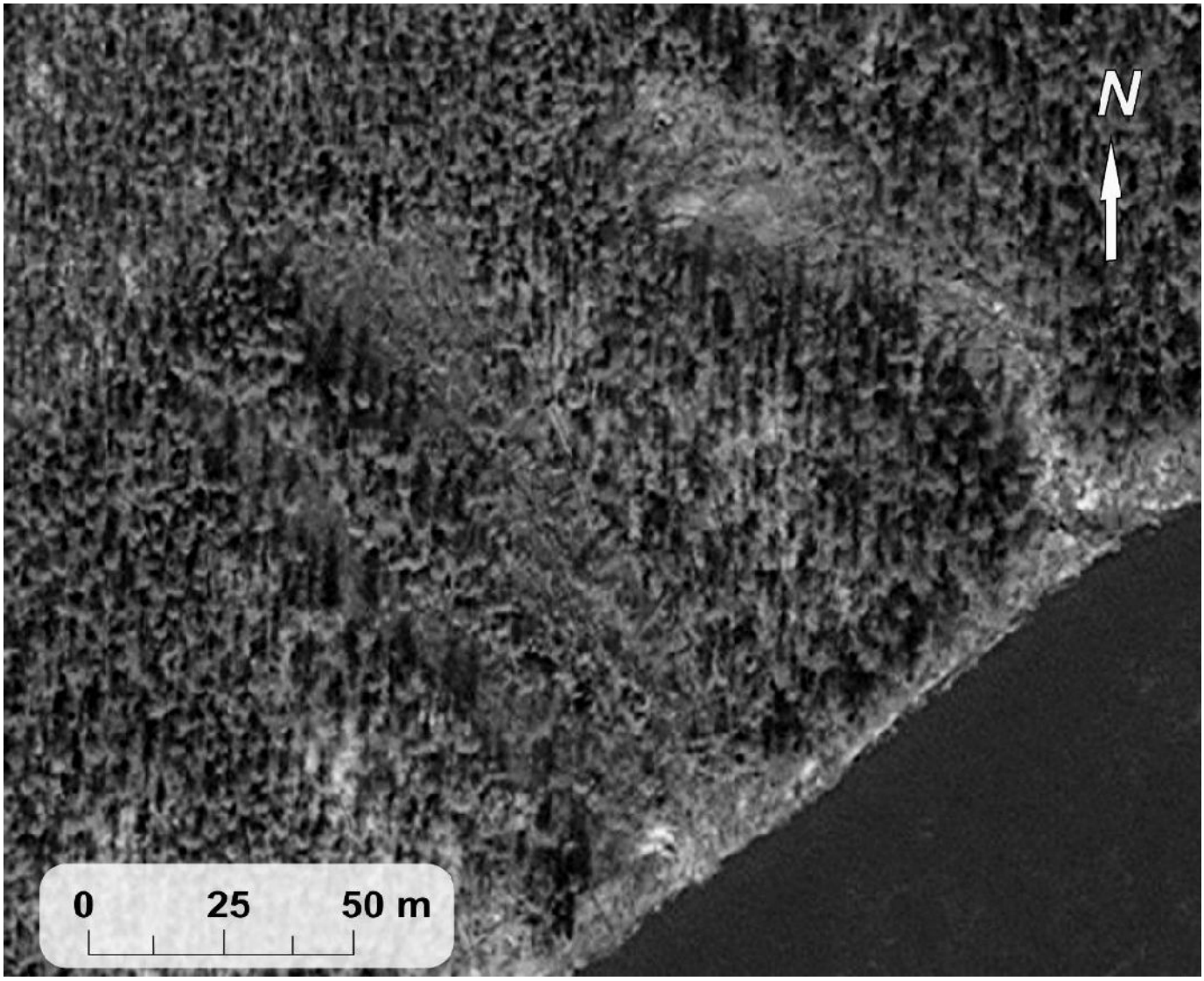

Figure A1. (No.2 in Table A1).

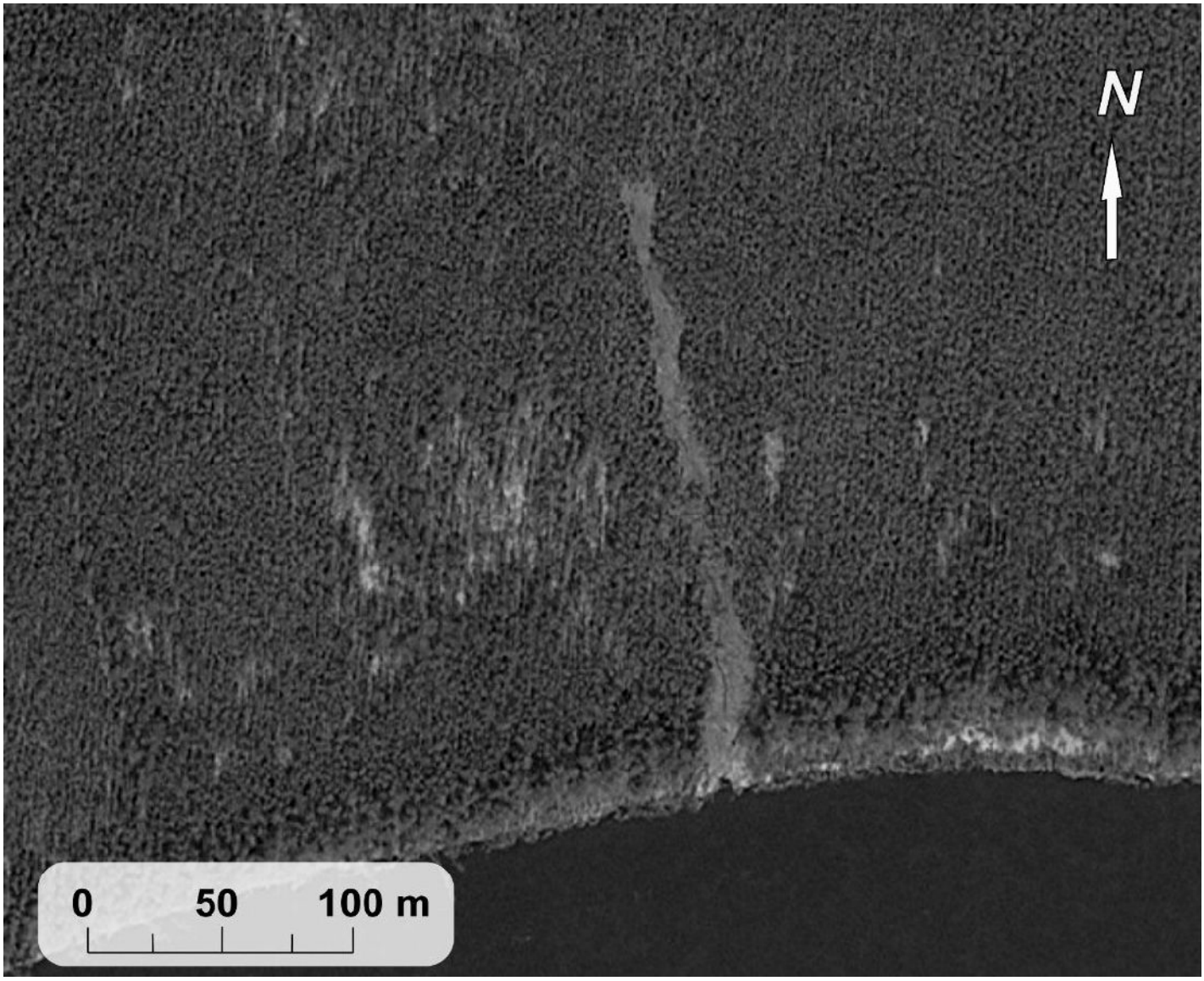

Figure A2. (No.18 in Table A1).

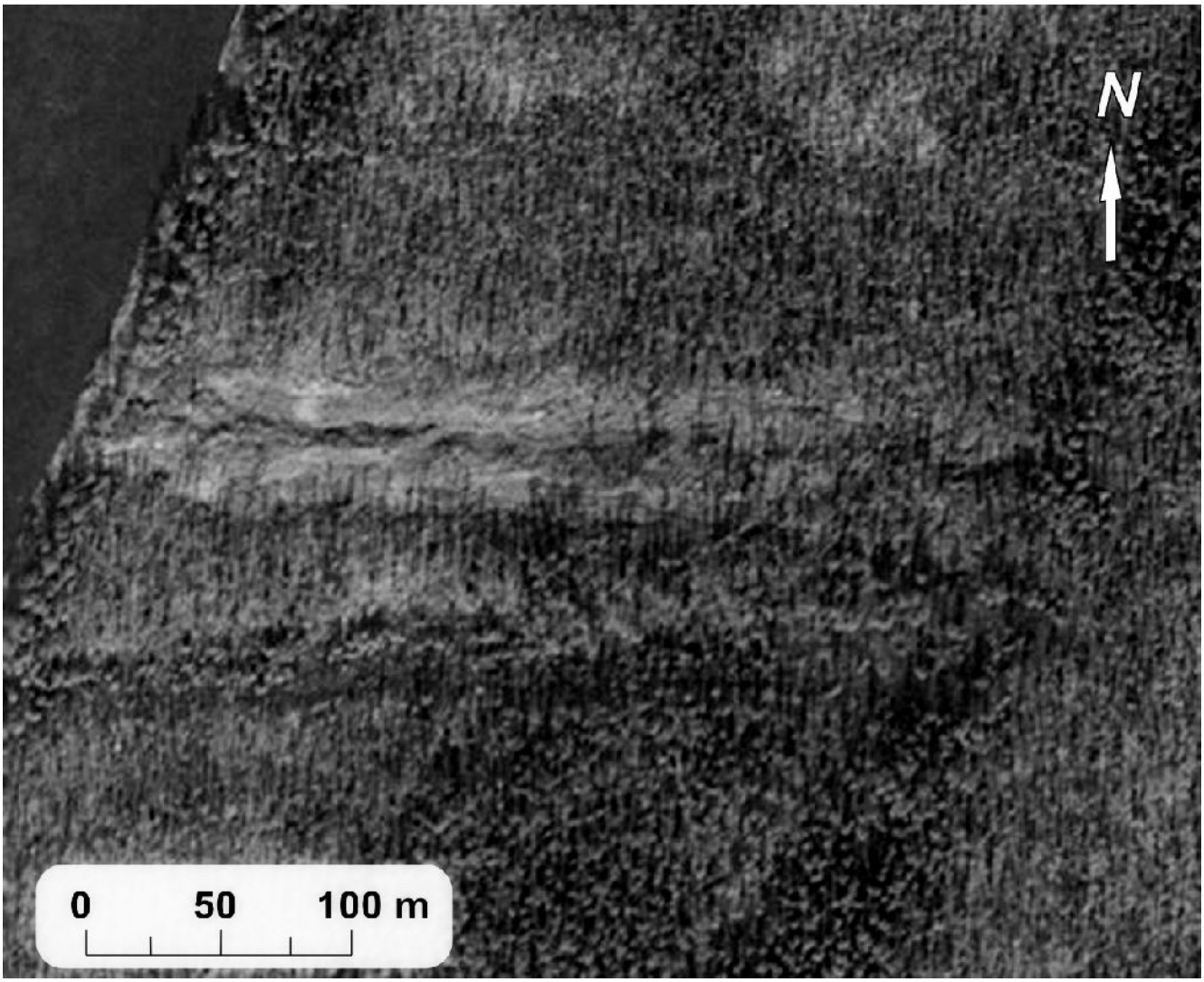

Figure A3. (No. 25 in Table A1).

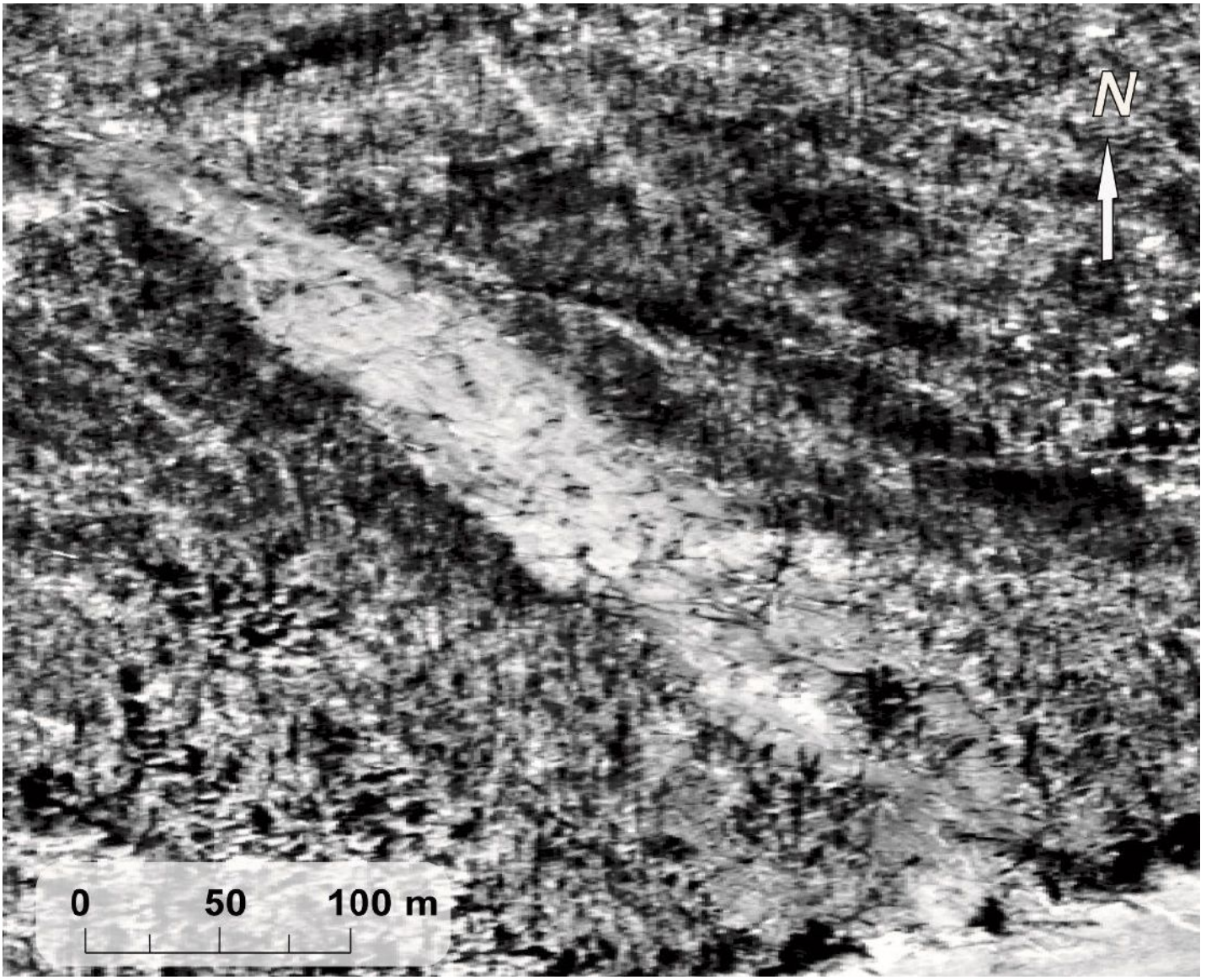

Figure A4. (No. 64 in Table A1).

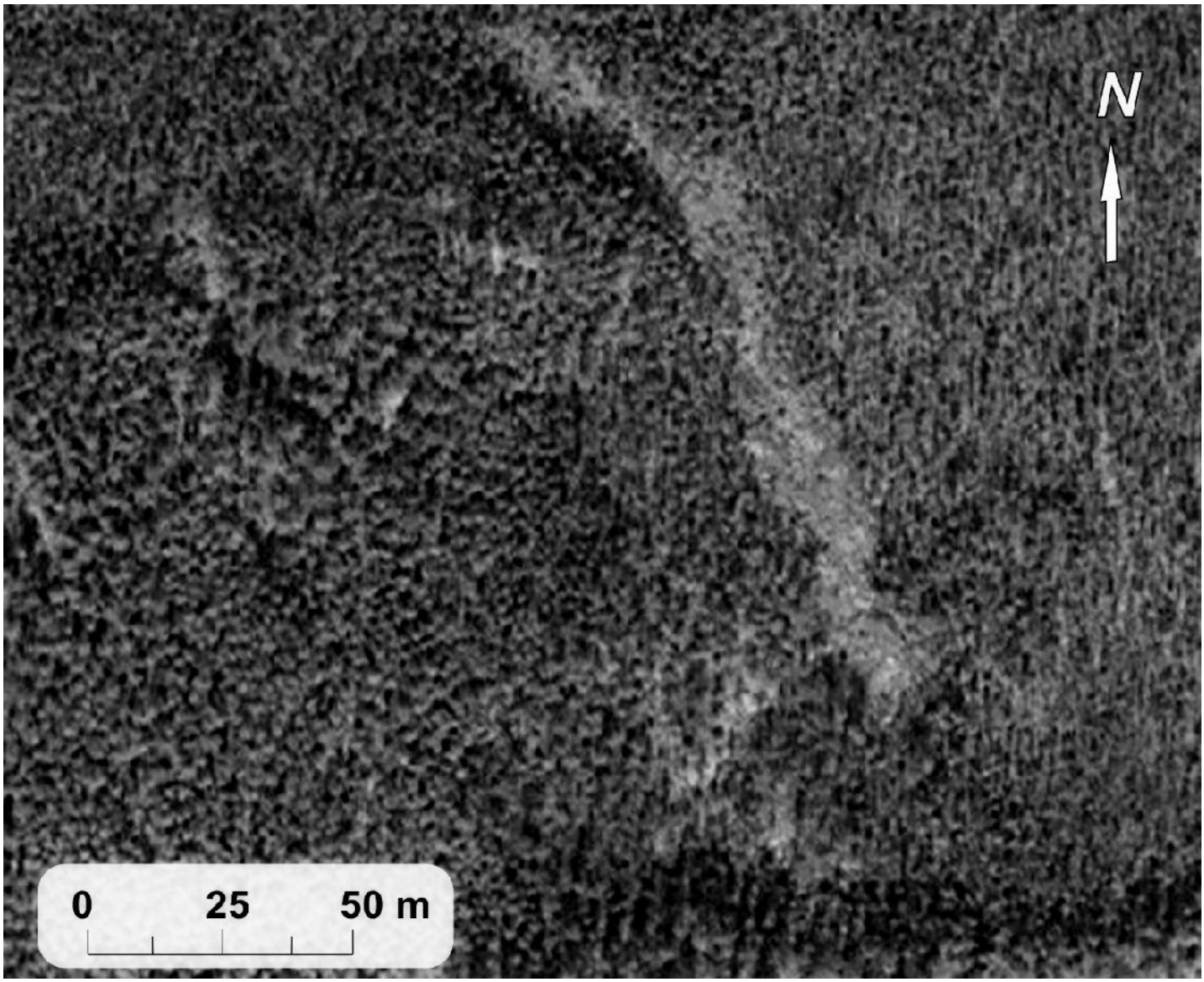

Figure A5. (No. 122 in Table A1).